AAC Accepted Manuscript Posted Online 11 June 2018
Antimicrob. Agents Chemother. doi:10.1128/AAC.00648-18

Biochemical and Structural Basis of Triclosan Resistance in a Novel Enoyl-Acyl Carrier Protein Reductase

Running title: Novel triclosan resistant enoyl ACP reductase

Raees Khan[a†], Amir Zeb[b†], Nazish Roy[a], Roniya Thapa Magar[a], Hyo Jeong Kim[a], Keun Woo Lee[b]#, Seon-Woo Lee[a]#

[a]*Department of Applied Bioscience, Dong-A University, Busan 49315, Republic of Korea*

[b]*Division of Applied Life Science (BK21 Plus Program), Plant Molecular Biology and Biotechnology Research Center (PMBBRC), Research Institute of Natural Science (RINS), Gyeongsang National University, Jinju 52828, Republic of Korea*

#Address correspondence to Seon-Woo Lee, seonlee@dau.ac.kr and to Keun Woo Lee kwlee@gnu.ac.kr

[†]These authors contributed equally to this work.

ABSTRACT

Enoyl-acyl carrier protein reductase (ENR), such as FabI, FabL, FabK and FabV, catalyzes the last reduction step in bacterial type II fatty acid biosynthesis. Previously, we reported metagenome-derived ENR homologs resistant to triclosan (TCL) and highly similar to 7-α hydroxysteroid dehydrogenase (7-AHSDH). These homologs are commonly found in Epsilonproteobacteria, a class that contains several human pathogenic bacteria, including the genera *Helicobacter* and *Campylobacter*. Herein, we report the biochemical and predicted structural basis of TCL resistance in a novel 7-AHSDH-like ENR. The purified protein exhibited NADPH-dependent ENR activity but no 7-AHSDH activity, despite its high homology with 7-AHSDH (69%-96%). Because this ENR was similar to FabL (41%), we propose that this metagenome-derived ENR is referred to as FabL2. Homology modeling, molecular docking, and molecular dynamic simulation analyses revealed the presence of an extrapolated six-amino acid loop specific to FabL2 ENR, which prevented the entry of TCL into the active site of FabL2 and was likely responsible for TCL resistance. Elimination of this extrapolated loop via site-directed mutagenesis resulted in the complete loss of TCL resistance but not enzyme activity. Phylogenetic analysis suggested that FabL, FabL2, and 7-AHSDH diverged from a common short-chain dehydrogenase reductase family. This study is the first to report the role of the extrapolated loop of FabL2-type ENRs in conferring TCL resistance. Thus, the FabL2 ENR represents a new drug target specific for pathogenic bacteria of Epsilonproteobacteria.

INTRODUCTION

Enoyl-acyl carrier protein (ACP) reductase (ENR) catalyzes the last step of the bacterial type II fatty acid synthesis (FASII) cycle to reduce the enoyl-ACP to fully saturated acyl-ACP (Fig. 1A and 1B). NADH, NADPH, or reduced flavin mononucleotide ($FMNH_2$) function as coenzymes in this reduction reaction (1). A majority of the enzymes involved in the FASII cycle are relatively conserved among bacteria, except ENR (2). Till date, four prototypic bacterial ENR isozymes have been reported, including FabI (3), FabL (4), FabV (5), and FabK (6). Except for FabK, which is an FMN-containing protein, all ENR isozymes belong to the short-chain dehydrogenase reductase (SDR) superfamily (7). These ENRs share low sequence similarity (15%–30%), although their active sites and specific sequence motifs required for coenzyme binding are highly conserved (8–10).

Triclosan [5-chloro-2-(2,4-dichlorophenoxy)phenol] (TCL) is a broad-spectrum antimicrobial that targets ENR of various organisms, thereby blocking FASII and ultimately preventing microbial growth (11). For years, TCL has been incorporated in a variety of consumer and personal care products worldwide (12–14) because of its potential antimicrobial activity. However, TCL resistance is prevalent among bacteria, and various mechanisms have been proposed as the basis for this resistance, including high ENR expression (15), mutant ENR versions tolerant to TCL (16), cell membrane modifications (17), various efflux pumps (15, 18), TCL-degrading enzymes (19), novel ENRs, and other unknown TCL resistance determinants (20). Additionally, TCL has been known to impose selective pressure on bacterial pathogens, thereby inducing co- or cross-resistance to other antibiotics (16, 20–25). Furthermore, there are increasing concerns regarding the excessive use of TCL and its negative effects on the environment and public health (12, 13).

FabI is known as the only effective ENR target for TCL, although substitutions of various key amino acid residues in FabI result in significant TCL resistance (20, 26–28). FabK has been reported to confer either low (20) or high resistance to TCL (6), whereas other ENRs such as FabL confer low resistance, and FabV (5), 7-α hydroxysteroid dehydrogenase (7-AHSDH)-like ENR homologs, and FabG-like ENR homologs confer high resistance to TCL (20). Being pivotal for bacterial survival and growth, ENRs have been used as potential targets for various antimicrobials for decades, and various synthetic ENR inhibitors have either been marketed or are currently being developed or in trial (29).

Previously, we identified a novel, TCL-tolerant, 7-AHSDH-like protein homolog (KT982367.1; AOR51268.1) from soil metagenome, which complements ENR activity in a conditional *Escherichia coli* mutant JP1111 (*fabI*^{ts}) and renders the bacteria completely tolerant to TCL (20). The gene encoding this 7-AHSDH-like protein is of special interest, as it is present in Epsilonproteobacteria, a class that contains many bacterial pathogens of humans, including *Helicobacter pylori* and *Campylobacter jejuni* (20). The gene encoding the 7-AHSDH-like homolog from *H. pylori* and *C. jejuni* has been shown to confer TCL resistance in *E. coli* (20). In the present study, we aimed to determine whether the 7-AHSDH-like protein possesses dual enzymatic activity of ENR and 7-AHSDH and its role in TCL resistance. Based on phylogenetic analysis, biochemical characterization, and molecular simulation, the 7-AHSDH-like enzyme showed divergent evolution from the SDR family, with a unique TCL resistance mechanism. We propose that this 7-AHSDH-like enzyme be referred to as FabL2. Because the FabL2-type ENRs are commonly found along with FabI type ENRs (30) in the pathogenic bacterial group of Epsilonproteobacteria, FabL2 has significant implications in healthcare and drug discovery.

MATERIALS AND METHODS

Bacterial strains, plasmids, culture condition, and general DNA manipulation

The *E. coli* strains DH5α, EPI300, and BL21 (DE3) were grown at 37°C in Luria–Bertani (LB) broth or on LB agar media containing appropriate antibiotics: TCL (1–600 µg/ml; Sigma–Aldrich Co., St. Louis, MO, USA), chloramphenicol (50 µg/ml), ampicillin (100 µg/ml), or kanamycin (50 µg/ml). Recombinant DNA manipulation was performed as previously described (31). Oligonucleotide synthesis and DNA sequencing were conducted at the DNA sequencing facility of MacroGen (Seoul, Korea). Nucleotide and amino acid sequences were compared using the online version of BLAST and ORF finder, publicly available at the National Center for Biotechnology Information portal (NCBI; http://blast.ncbi.nlm.nih.gov). Multiple sequence alignments were performed using BioEdit v7.2.5 and GeneDoc v2.7 software.

Phylogenetic analysis

Phylogenetic analysis was performed as previously described (20) for metagenomic FabL2 ENR using amino acid sequences of FabL2 and its homologs, prototypic FabL, FabI, FabV, FabK ENRs, and prototypic 7-AHSDH from *Comamonas testosteroni* and its homologs retrieved from the UniRef50 database (updated on September 19, 2017). Top 10 entries were selected from each homology search. All identified sequences compiled together with the closely related prototypic ENRs and metagenomic FabL2, and redundant sequences were removed using the online Decrease Redundancy program (32). Sequence alignment and phylogenetic tree construction were performed with MEGA 6 (33) using the MUSCLE algorithm (34). To analyze the alignment output in MEGA 6, the maximum likelihood method was used in combination with the nearest-neighbor-interchange strategy, resulting in the

deletion of gaps present in less than 50% of the sequences and generating 500 bootstrapped replicates resampling data sets to evaluate the confidence.

Expression and purification of FabL2 ENR

A gene encoding FabL2 ENR was PCR amplified from pBF1-4 (20) using gene-specific forward primer (5′-ATTCAAGGATCCTAGAGACATGACAAATATGAAAGGCAA-3′) and reverse primer (5′-TTATCATCTTTTAACATATAATAGATGGTCGACTTTCAA-3′) containing *Bam*HI and *Sal*I restriction sites, respectively. The amplified PCR product was digested with *Bam*HI and *Sal*I restriction endonucleases and cloned into pET-30b(+) expression vector to generate the recombinant vector, pEBF1-4.

To express the FabL2 protein, pEBF1-4 was transformed into *E. coli* BL21 (DE3) cells, and recombinant cells were selected on LB agar medium containing kanamycin. *E. coli* cells carrying pEBF1-4 were grown in 200 ml of LB supplemented with kanamycin at 37°C until reaching an optical density of 0.5 at 600 nm (OD_{600}). To induce protein expression, isopropyl β-D-1-thiogalactopyranoside (IPTG) (1 mM) was added to the bacterial culture during the late exponential phase. For protein purification, *E. coli* cells were harvested, re-suspended in 5 ml of binding buffer [20 mM Tris-Cl, 0.5 M NaCl, 40 mM Imidazole, (pH 8.0)], and subjected to sonication (Sonic Dismembrator Model 500; Fisher Scientific) for 2 min (pulse ON: 5 s, pulse OFF: 10 s). This mixture was then centrifuged at 3,500 × *g* for 6 min at 25°C. The supernatant was collected and re-centrifuged at 17,000 × *g* for 10 min at 25°C and filtered using a 0.45-µm membrane filter. The fusion protein was purified using AKTA prime liquid chromatography system (GE Healthcare, Buckinghamshire, UK) with His Trap™ HP affinity column (1 ml bed

volume; GE Healthcare). The identity of the purified fusion protein was confirmed by denaturing sodium dodecyl sulphate-polyacrylamide gel electrophoresis (SDS-PAGE).

Analysis of FabL2 enzymatic activity

While the deduced amino acid sequence of FabL2 showed high sequence similarity to that of 7-AHSDH, *fabL2* has previously shown to complement the ENR mutant *E. coli* (20). To test if FabL2 possesses dual enzymatic activity, enzyme assays were performed using the purified fusion protein. Biochemical characterization of the purified fusion protein was performed to determine the optimum reaction conditions and Michaelis–Menten kinetics for ENR activity. All enzyme assays were performed as previously described (35) with slight modifications. Briefly, ENR activity was measured in a 100-µl volume containing NADH/NADPH cofactors (250 µM), crotonyl-coenzyme A (CoA) substrate (200 µM), FabL2 protein (450 nM), and sodium phosphate buffer (100 mM; pH 7.0) at 25°C. Crotonyl-CoA, NADH, and NADPH were purchased from Sigma–Aldrich. Enzymatic reactions were monitored using the UV/Vis Spectrophotometer (DU730 Life Science; Beckman Coulter Inc., Fullerton, CA, USA) at 340 nm and 30-s intervals for a total of 3 min. Because the protein did not exhibit ENR activity with NADH and preferred NADPH as a cofactor, the latter was used in all subsequent enzyme assays. To determine the value of the Michaelis–Menten constant (Km) of the protein, 100 nM of purified protein was added to 100 µl of the reaction mixture containing 200 µM NADPH and varying concentrations of crotonyl-CoA (3, 6, 12, 24, 36, and 48 µM). To determine the Km value of NADPH, 100 nM of protein was added to 60 µM of crotonyl-CoA and varying concentrations of NADPH (5, 10, 15, 20, 30, 50, and 75 µM). The oxidation of NADPH cofactor was spectrophotometrically measured at 340 nm. The reaction mixtures were incubated at 25°C

for 10 min. To determine the optimal buffer composition and pH for enzymatic activity of the protein, reactions were conducted using different buffers over a wide pH range: 100 mM sodium citrate buffer (pH 3.2, 4.2, 5.2, and 6.2) and 100 mM sodium phosphate buffer (pH 6.5, 7, 7.5, and 8.0). To determine whether FabL2 possessed 7-AHSDH activity, enzyme assays were performed using cholic acid (Sigma–Aldrich) as the substrate and NADH and NADPH as cofactors, as previously described (36). All kinetic reactions were performed in triplicates. The initial velocity of the reaction was calculated from the linear phase of the progress curves. To calculate the Km values both for the substrate and cofactor, data were fitted to the standard Michaelis–Menten equation.

Site-directed mutagenesis

Sequence comparison, homology modeling, and docking analysis revealed that FabL2-type ENR carries an extrapolated highly flexible loop comprising six amino acid residues (Y96–V101); this was specific to FabL2 ENR only, as other known ENRs lack this loop. To test if this extrapolated flexible loop was involved in TCL resistance and enzymatic activity, overlap extension PCR was used to delete the 18-bp loop (Fig. S1, region b). Briefly, two PCRs were performed to amplify the overlapping fragments A and C of the *FabL2* gene (Fig. S1) from pBF1-4 using the primer pairs 7A-1/A-2 (7A-1: 5′-GCCAAAGCGTTGTCAGGTG-3′ and 7A-2: 5′-<u>AATCATCGCATTGCTTACGA</u>AG-3′) and 7A-3/A-4 (7A-3: 5′-<u>TCGTAAGCAATGCGATGATT</u>GGCGGATACGGTAAATTTAT-3′ and 7A-4: 5′-CCCGTCATATTACTCGTTCCCA-3′), respectively. The PCR conditions were as follows:

181 initial denaturation at 95°C for 3 min, 30 cycles of denaturation at 95°C for 30 s, annealing at
182 variable temperatures (55°C or 63°C for the amplifying fragment A or C, respectively) for 30 s,
183 and extension at 72°C for 30 s, followed by a final extension at 72°C for 5 min. The amplified
184 PCR products A and C were gel-purified. This was followed by a fusion PCR using fragments A
185 and C as templates in equimolar concentrations without any primers and the following conditions:
186 initial denaturation at 95°C for 3 min, 10 cycles of denaturation at 95°C for 1 min, annealing at
187 50°C for 30 s, and extension at 72°C for 1 min 35 s, followed by a final extension at 72°C for 5
188 min. The fusion product was subsequently amplified using 7A-1 and 7A-4 primers (Fig. S1) and
189 the following conditions: initial denaturation at 95°C for 3 min, 20 cycles of denaturation at
190 95°C for 1 min, annealing at 63°C for 30 s, and extension at 72°C for 1 min 35 s, followed by a
191 final extension at 72°C for 5 min. The purified fusion product was cloned into the pGEM-T Easy
192 vector and transformed into *E. coli* DH5α to confirm the deletion of the loop and test for TCL
193 resistance as previously described (20). The mutated version of *FabL2* was designated as
194 *mFabL2*.
195
196 **Complementation**
197 To investigate the ENR activity of mFabL2, complementation studies were performed. The
198 recombinant pGEM-T Easy plasmid carrying *mFabL2* was transformed into the conditional
199 temperature-sensitive *fabI* mutant of *E. coli*, JP1111, which is unable to grow at a high
200 temperature of 42°C (37). *E. coli* JP1111 containing the *mFabL2* vector were grown in triplicates
201 on LB agar medium supplemented with ampicillin (100 µg/ml) and IPTG at 30°C and 42°C. The
202 growth of *E. coli* JP1111 at 42°C for 48 h indicated complementation of FabI ENR activity.
203

TCL resistance test

To determine and compare the growth and TCL resistance of *E. coli* DH5α expressing either metagenomic FabL2 or mFabL2, growth assays were performed in LB broth supplemented with ampicillin and various concentrations of TCL (0–600 µg/ml). *E. coli* DH5α expressing *Bacillus velezensis* FabL homolog (WP_003155478.1) was used as a positive control at similar TCL concentrations, and *E. coli* DH5α carrying empty pGEM-T Easy vector was used as a negative control. Bacterial growth was monitored using UV/Vis Spectrophotometer (DU730 Life Science; Beckman Coulter Inc., Fullerton, CA, USA) by measuring OD_{600} over 96 h.

Homology modeling of FabL2

Homology modeling is the construction of an atomic model of the target protein utilizing experimentally determined structures of evolutionarily-related proteins (38). First, the FabL2 protein sequence (target) was analyzed against the Protein Data Bank (PDB) using the *BLASTP* tool in NCBI to identify the suitable protein structure (template) (https://blast.ncbi.nlm.nih.gov/Blast.cgi?PROGRAM=blastp&PAGE_TYPE=BlastSearch). Subsequently, the target–template alignment was subjected to MODELLER program implemented in Discovery Studio v4.5. Ten iterative models of FabL2 were generated, and the best model was selected based on the lowest probability density function (PDF) total energy and discrete optimized protein energy (DOPE) score for further analysis.

It is noteworthy to mention that the homology model does not reflect the conformation or orientation of amino acids comprising side chains in their physiological state. To obtain the native conformation of FabL2, an unrestrained molecular dynamic (MD) simulation was

227 performed with CHARMm36 force field in GROMACS v5.0.7 (39). Briefly, the system was
228 solvated in an octahedral box of transferable intermolecular potential three position (TIP3P)
229 water model. Counter-ions (Na^+) were added to neutralize the system. The steepest descent
230 minimization with a maximum tolerance of 10 kJ/mol/nm was employed to avoid any
231 unfavorable interactions. The system was equilibrated in two phases. In the first phase, NVT
232 equilibration was conducted for 100 ps at 300 K. The temperature was maintained with a V-
233 rescale thermostat. In the second phase, heavy atoms were restrained, and solvent molecules with
234 counter-ions were allowed to move during the 100-ps simulation at 300 K and 1.0 bar pressure
235 using the Parrinello–Rahman barostat. The final production step was conducted for 10 ns under
236 periodic boundary conditions with NPT ensemble and bond constraint algorithm, linear
237 constraint solver (LINCS). The representative structure of FabL2 was extracted from the last 6-
238 ns trajectory using the clustering method. The stereochemical quality of the MD-refined model
239 of FabL2 was verified using PROCHECK implemented in SAVES web server
240 (http://services.mbi.ucla.edu/PROCHECK/). The MD-refined model of FabL2 was also validated
241 by ProSA-web (https://prosa.services.came.sbg.ac.at/prosa.php) for its accuracy of potential
242 errors. The Z-score of ProSA measures the deviation of the total energy of the structure with
243 respect to an energy distribution derived from random conformations.
244

245 **Molecular docking simulation of TCL into FabL2**

246 Molecular docking is a computational technique used to predict the binding affinity and
247 orientation of a ligand in the binding site of a protein. The two-dimensional (2D) structure of
248 TCL was drawn in Accelrys Draw v4.2 and converted into three-dimensional (3D) structure in
249 Discovery Studio v4.5. The MD-refined model of FabL2 and TCL were used as input data in

Genetic Optimization of Ligand Docking (GOLD) v5.2.2 program. The binding site of FabL2 was traced from its catalytic residues using *Define and Edit Binding Site* tools implemented in Discovery Studio v4.5. Docking results were analyzed with the GOLD fitness score that includes hydrogen bond (H-bond) energy, van der Waals energy, and ligand torsion strains. The best docking pose was selected based on the GOLD fitness score and H-bonding with catalytic residues.

Accession number(s)

The nucleotide sequence of pBF1 harboring the *FabL2* gene has been deposited in the GenBank database under the accession number KT982367. The FabL2 ENR protein sequence has been deposited in the GenBank database under the accession number AOR51268.1.

RESULTS AND DISCUSSION

Phylogenetic analysis of FabL2, 7-AHSDH-like protein, and prototypic ENRs

ENR catalyzes the final reduction step in the bacterial FASII cycle and is indispensable for establishing and maintaining the rate of fatty acid biosynthesis (40, 41). Amino acid sequence analysis revealed that FabL2 shared significant homology (69%-96%) with the 7-AHSDH homologs of Epsilonproteobacteria and relatively less similarity with FabL (41%), FabI (27%), and prototypic 7-AHSDH (34%) (20). Moreover, FabL2 ENR shared similar structural features such as highly conserved tyrosine and lysine residues of the active site with prototypic FabI and FabL ENRs. Similarly, key residues of the enzyme such as Ser146, Lys163, Thr193 and RINA like sequences were strictly conserved among the FabL2 ENR and prototypic 7-α-HSDH (20).

Additionally, the FabL2 protein conferred complete TCL tolerance when expressed in *E. coli* and complemented the ENR activity in the *E. coli* mutant, JPP1111, carrying the *fabI*^{ts} mutation (20). Phylogenetic analysis of the FabL2 protein with other prototypic ENRs and 7-AHSDH proteins and their homologs revealed that FabL2-type ENRs clustered as a separate clade (Fig. 2), suggesting that FabL2 diverged from either closely related FabL and FabI ENRs or from 7-AHSDH during evolution. Therefore, we designated this enzyme as FabL2. Consequently, distinguishing these types of ENRs based only on sequence comparison/annotation is not always ideal (20).

NADPH-dependent ENR activity of the FabL2 protein

A fusion protein of FabL2 was purified and confirmed to be of expected size (33.56 kDa) using SDS-PAGE (Fig. S2A, S2B). The conversion of NADH/NADPH cofactors to NAD/NADP at 340 nm was monitored to assess the ENR activity. Because the purified protein exhibited maximum activity in 100 mM sodium phosphate buffer (pH 7.0) (Fig. S2C), all subsequent assays were performed using this buffer. No enzymatic activity was observed in 100 mM sodium citrate buffer regardless of the pH (data not shown). The purified protein catalyzed the turnover of NADPH (Km = 27.64 µM) (Fig. 3A) into NADP in the presence of crotonyl-CoA (Km = 9.627 µM) as a substrate (Fig. 3B). These Km values for the metagenomic ENR were equivalent to those reported for *Chlamydia trachomatis* and *E. coli* ENRs (4, 35), although these values were slightly lower than those reported by Ward *et al.* and Basso *et al*. (42, 43). The purified protein did not utilize NADH as a cofactor, thus, exhibiting ENR activity only with NADPH.

Among other prototypic ENRs, FabL from *B. subtilis* showed high similarity to FabL2 ENR (41%), which uses NADPH as a cofactor (4), whereas FabV using NADPH as a cofactor (1)

295 did not show any similarity to FabL2. The *kcat* values for FabL2 with NADPH (1.09 μM/min)
296 and crotonyl-ACP (0.18283 μM/min) (Table S1) were within the range reported previously (44)
297 but were lower than those for the ENR from *C. trachomatis* (35). These variations might be due
298 to the use of different substrates. Overall, biochemical analyses confirmed that FabL2 enzyme
299 possesses an NADPH-dependent ENR activity. However, despite its high similarity with 7-
300 AHSDH from Epsilonproteobacteria, FabL2 did not exhibit 7-AHSDH activity when tested with
301 cholic acid substrate and NADH and NADPH cofactors (data not shown). These data suggest
302 that the enzyme FabL2 from soil metagenome is a bona fide ENR similar to FabL.
303
304 **Predicted structure of FabL2**
305 Sequence analysis of metagenomic TCL-resistant FabL2 showed 41.0% sequence similarity with
306 FabL from *B. subtilis*. Sequence alignment revealed Gly102, Tyr160, Lys167, and Phe204 as the
307 catalytic residues of FabL2 (Fig. 4A) and an extrapolated loop to be tested for TCL resistance
308 (Fig. 4B) and ENR function (Fig. 4C). Therefore, the structure of FabL from *B. subtilis* (PDB ID:
309 3OID; chain A) was considered as template for homology modeling of FabL2. Among ten
310 predicted models, the best model of FabL2 was selected based on the lowest molecular
311 probability density function (MOLPDF) score of 1,414.23 and DOPE score of −26,020.47. The
312 representative structure of FabL2 was extracted after MD simulation refinement. The
313 stereochemical quality of the refined FabL2 structure revealed that 88.6% of the residues
314 occupied the most favored region of the Ramachandran plot (45) (Fig. S3A). These results
315 suggest that phi (ϕ) and psi (ψ) backbone dihedral angles in the modeled structure are reasonably
316 accurate. Analysis of FabL2 with ProSA-web (46) revealed a Z-score of −7.31, which was within
317 the range of Z-scores of experimentally determined structures (Fig. S3B).

The MD-refined structure of FabL2 has an architecture similar to that reported for FabL proteins (47). Briefly, the overall structure of FabL2 comprises a central 7-stranded parallel β-sheet (β1–β7) sandwich-like structure flanked on both sides by three α-helices, forming an NADPH-binding Rossman-like fold (48) (Fig. 5A). Our modeled FabL2 structure also exhibited the same folding pattern in the substrate-binding region (α8 and α9) located near the carboxyl end of β6 and β7 as previously described for different ENRs and other members of the SDR family (4, 49, 50). Despite the high similarity of FabL2 with FabL from *B. subtilis*, FabL2 contained an extrapolated region extending between Tyr96 and Val101 residues (Fig. 4A, Fig. 5A and 5B). The structural superimposition of FabL2 and FabL affirmed that the extrapolated six amino acid residues formed a loop (Fig. 5A, orange color). The role of this loop in substrate specificity and TCL resistance of FabL2 was subsequently validated.

Interaction of TCL with FabL2

The best docking pose of TCL with FabL2 revealed a GOLD fitness score of 53.00. Despite the high docking score, TCL was flipped away (~5.7 Å) from the catalytic site of FabL2 and was bound at the rim region of the tunnel leading to the substrate-binding site (Fig. 5B). Furthermore, despite the phenol moiety, the phenoxy group of TCL was oriented toward the catalytic pocket of FabL2. Molecular interactions between FabL2 and TCL implied that the Arg98 residue of the extrapolated loop formed two H-bonds with the backbone oxygen and phenolic oxygen of TCL (Fig. 5C). Moreover, other non-polar interactions confirmed the binding of TCL at the rim region of the tunnel leading to the catalytic site of FabL2 (Fig. 5C). Our rational approach concluded that TCL could not reach the catalytic site of FabL2 due to H-bonding with Arg98 and other non-polar interactions (Fig. 5A and 5B). This flexible loop may determine the shape and size of the

tunnel. We further speculate that the extrapolated loop is highly flexible and plays a key role in TCL resistance of FabL2.

Based on our results, we hypothesized that removing this extrapolated flexible loop (Tyr96–Val101) from FabL2 renders it sensitive to TCL. To test this hypothesis, we created mutant FabL2 (mFabL2) lacking the extrapolated loop and predicted its structure as previously described for FabL2 (Fig. 4B). The best model had the lowest PDF and DOPE scores of 1,353.46 and −24,680.74, respectively. PROCHECK analysis of mFabL2 revealed that 92.6% of amino acid residues occupied the most favored region of the Ramachandran plot (Fig. S3C). The Z-score of mFabL2 model was −6.74, which followed the Z-score pattern of wild-type FabL2 (Fig. S3D). Both FabL2 and mFabL2 showed a similar overall topology and model quality, except for the tunnel leading to catalytic cavity (Fig. 5D). Based on these data, we speculate that the native function of mFabL2 was unaffected by the deletion of the flexible loop.

Although the docking score of mFabL2 was the same as that of the wild-type FabL2 (53.00), TCL occupied the catalytic active site of mFabL2. The binding of TCL with mFabL2 was similar to that observed with other ENR family members with respect to the orientation of the phenol moiety toward the substrate-binding site (Fig. 5E). Moreover, the H-bonding between TCL and Tyr154 of mFabL2 stabilized its orientation in the active site of mFabL2 (Fig. 5F). Further, the H-bonding between amino acid residues of mFabL2 and NADPH generate stable enzyme complex of mFabL2 (Fig. 5G). This binding pattern of TCL is conserved across all ENR family members (28, 47, 51, 52).

MD simulation of the mFabL2-TCL complex

363 Detailed analysis of the binding mode of TCL with the active site of mFabL2 was conducted via
364 20-ns MD simulation. The root mean square deviation (RMSD) of the C_α atoms (Fig. 5H), the
365 simulation of the mFabL2-TCL complex (Fig. 5I) and analysis of molecular interactions (Fig. 5J,
366 Fig. S4A and S4B) indicated that the system remained stable during the entire simulation period.
367 This mechanism of targeting the catalytic Tyr by TCL is well documented among other ENR
368 family members (28, 47, 52). Our analysis also revealed an additional interaction between
369 NADPH and TCL via H-bonding (Fig. S4A and S4B), which may strengthen the binding of TCL
370 with mFabL2. Moreover, other molecular interactions, including π-π, alkyl-alkyl, π-alkyl, and
371 van der Waals interactions were observed between the catalytic site residues of mFabL2 and
372 TCL (Table S2, Fig. 5G). Taken together, these data validated our hypothesis and revealed that
373 the deletion of the extrapolated residues did not disturb the native folding of mFabL2 and restore
374 its sensitivity to TCL. Experimental validation confirmed the native function of mFabL2 as well
375 as its inhibition by TCL.
376
377 **The extrapolated loop of FabL2 is involved in TCL resistance**
378 Bioinformatics analysis revealed that the FabL2 has an extra six-residue loop (Tyr96–Val101),
379 which was specific to and supposed to be involved in TCL tolerance. These six residues extend
380 the loop dramatically, which pushes the Gly102 (conserved catalytic residue) away, creating a
381 new topology of the TCL-binding site of FabL2. We speculate that Arg98, which is sequestered
382 between Gly102 and TCL, interferes with their binding. Moreover, docking analysis of mFabL2
383 revealed that TCL is able to access the active site of mFabL2. Therefore, we conclude that the
384 Tyr96–Val101 loop is responsible for the observed TCL tolerance of FabL2; its removal may
385 result in the loss or reduction of TCL resistance. As expected, deletion of the Tyr96–Val101 loop

386 via site-directed mutagenesis resulted in the loss of TCL resistance in mFabL2 (minimum
387 inhibitory concentration, 2.5 µg/ml), whereas the wild-type FabL2 was capable of conferring
388 resistance to TCL even at concentrations as high as 600 µg/ml (Fig. S5A and S5B). Moreover,
389 complementation analysis revealed that mFabL2 retained its ENR activity (Fig. 4 C). This result
390 indicates that the Tyr96–Val101 loop is involved in TCL tolerance but not in ENR activity. The
391 strict amino acid conservation of this extrapolated loop (Fig. S6A) suggests that the loop was
392 recently introduced into FabL2 of Epsilonproteobacteria.

393 The extrapolated loop is highly unique and is present only in FabL2-type ENR and its
394 homologs in Epsilonproteobacteria; it is absent in the closely related prototypic FabL-type ENRs
395 and prototypic 7-AHSDH homologs (Fig. S6A, Fig. S6B, Table S3). It is unclear how and why
396 these enzymes have evolved to contain this extrapolated loop. However, this extrapolated loop
397 (Tyr96 – Gly102) in FabL2 is involved in the topology of tunnel leading to the enzyme active
398 site. The residues of the target loop are not considered as catalytic moieties of ENR, since
399 removal of the loop did not affect ENR activity. Although we have not tested specific point
400 mutation of the extrapolated loop, we speculate that specific point mutation of the loop would
401 not alter the overall structure of the loop. Our rational approach suggested that extrapolated loop
402 is highly flexible and fluctuates back and forth to open and close the opening of the tunnel
403 leading to the active site of FabL2 (Fig. 5A). However, this prediction still awaits further
404 biochemical investigation.

405 Our docking analysis of TCL into the active site of FabL2 suggested that TCL is flipped
406 away from docking site by ~5.7 Å, and hence TCL could not reach the catalytic site. If we delete
407 this loop, the main entrance of the tunnel will remain opened and TCL would be able to reach the
408 active site of FabL2. In fact, deletion of extrapolated loop could successfully abolish TCL

resistance in mFabL2. Finally, we perceived that extrapolated loop of FabL2 serves as a checkpoint to selectively allow substrate(s) to reach the active site, which needs to be further verified by structural characterization. Taken together, this study showed that minor changes in the structure of bacterial proteins due to small-scale structural variations in the coding sequence can render the bacteria resistant to antibiotics.

CONCLUSIONS

We conclude that FabL2 ENR confers complete TCL tolerance via a unique extrapolated loop in its protein structure. This study is the first to report TCL tolerance conferred by residues other than those directly interacting with the substrate or cofactor. Furthermore, the presence of TCL-resistant FabL2 ENR homologs among the human pathogenic bacteria of the Epsilonproteobacteria class indicates that these bacteria may be unaffected by TCL treatment. Additionally, although the amino acid sequence of FabL2 was highly similar to that of 7-AHSDH, the lack of 7-AHSDH activity in FabL2 indicates that sequence alignments alone are not sufficient for determining protein function.

Acknowledgements

This research was supported by a grant from the Next-Generation BioGreen 21 Program to S.-W. L. (Project No. PJ01313101) through Rural Development Administration and the Pioneer Research Center Program to K.W. L. (NRF-2015M3C1A3023028) through the National Research Foundation of Korea funded by the Ministry of Science, ICT and Future Planning, Republic of Korea.

Transparency declaration

None to declare.

Author contributions

S. W. L., R. K., K.W.L. and A.Z developed the framework for evaluating TCS resistance of the novel FabL2 type ENR. S.W.L. and K.W.L conceived, organized, and supervised the project. R. K., A.Z., K.W.L. and S. W. L. interpreted the results and prepared the manuscript. R. K., N.R., R.T.M. and H.J.K. performed experiments and analyzed the data. All authors contributed to the final version of the manuscript. The guarantor is S.W. L.

References

1. Massengo-Tiassé RP, Cronan JE. 2009. Diversity in enoyl-acyl carrier protein reductases. Cell. Mol. Life Sci. 66:1507–1517.
2. Jackowski S, Murphy CM, Cronan JE, Rock CO. 1989. Acetoacetyl-acyl carrier protein synthase. A target for the antibiotic thiolactomycin. J. Biol. Chem. 264: 7624–7629.
3. Bergler H, Wallner P, Ebeling A, Leitinger B, Fuchsbichler S, Aschauer H, Kollenz G, Högenauer G, Turnowsky F. 1994. Protein EnvM is the NADH-dependent enoyl-ACP reductase (FabI) of *Escherichia coli.* J. Biol. Chem. 269:5493–5496.
4. Heath RJ, Su N, Murphy CK, Rock CO. 2000. The enoyl-[acyl-carrier-protein] reductases FabI and FabL from *Bacillus subtilis*. J. Biol. Chem. 275:40128–40133.
5. Massengo-Tiassé RP, Cronan JE. 2008. *Vibrio cholerae* FabV defines a new class of enoyl-acyl carrier protein reductase. J. Biol. Chem. 283:1308–1316.

454 6. Heath RJ, Rock CO. 2000b. Microbiology: A triclosan-resistant bacterial enzyme. Nature
455 406:145–146.

456 7. White SW, Zheng J, Zhang YM, Rock CO. 2005. The structural biology of type II fatty acid
457 biosynthesis. Annu. Rev. Biochem. 74:791–831.

458 8. Joernvall H, Persson B, Krook M, Atrian S, Gonzalez-Duarte R, Jeffery J, Ghosh D. 1995.
459 Short-chain dehydrogenases/reductases (SDR). Biochemistry 34:6003–6013.

460 9. Kallberg Y, Oppermann U, Jörnvall H, Persson B. 2002. Short-chain
461 dehydrogenases/reductases (SDRs). Eur. J. Biochem. 269:4409–4417.

462 10. Persson B, Kallberg Y, Oppermann U, Jörnvall H. 2003. Coenzyme-based functional
463 assignments of short-chain dehydrogenases/reductases (SDRs). Chem. Biol. Interact.
464 143:271–278.

465 11. Heath RJ, Rubin JR, Holland DR, Zhang E, Snow ME, Rock CO. 1999. Mechanism of
466 triclosan inhibition of bacterial fatty acid synthesis. J. Biol. Chem. 274:11110–11114.

467 12. Halden RU. 2014. On the need and speed of regulating triclosan and triclocarban in the
468 United States. Environ. Sci. Technol. 48:3603–3611.

469 13. Yueh MF, Tukey RH. 2016. Triclosan: a widespread environmental toxicant with many
470 biological effects. Annu. Rev. Pharmacol. Toxicol. 56:251–272.

471 14. Saleh S, Haddadin RN, Baillie S, Collier PJ. 2011. Triclosan–an update. Lett. Appl.
472 Microbiol. 52:87–95.

15. Yazdankhah SP, Scheie AA, Høiby EA, Lunestad BT, Heir E, Fotland TØ, Naterstad K, Kruse H. 2006. Triclosan and antimicrobial resistance in bacteria: an overview. Microb. Drug Resist. 12:83–90.

16. McMurry LM, McDermott PF, Levy SB. 1999. Genetic evidence that InhA of *Mycobacterium smegmatis* is a target for triclosan. Antimicrob. Agents Chemother. 43:711–713.

17. Russell AD. 2004. Whither triclosan? J. Antimicrob. Chemother. 53:693–695.

18. McMurry LM, Oethinger M, Levy SB. 1998b. Overexpression of *marA*, *soxS*, or *acrAB* produces resistance to triclosan in laboratory and clinical strains of *Escherichia coli*. FEMS Microbiol. Lett. 166:305–309.

19. Lee DG, Zhao F, Rezenom YH, Russell DH, Chu KH. 2012. Biodegradation of triclosan by a wastewater microorganism. Water research 6:4226-4234.

20. Khan R, Kong HG, Jung YH, Choi J, Baek KY, Hwang EC, Lee SW. 2016. Triclosan resistome from metagenome reveals diverse enoyl acyl carrier protein reductases and selective enrichment of triclosan resistance genes. Sci Rep. 6:1–13.

21. Fernando DM, Xu W, Loewen PC, Zhane GG, Kumar A. 2014. Triclosan can select for an AdeIJK-overexpressing mutant of *Acinetobacter baumannii* ATCC 17978 that displays reduced susceptibility to multiple antibiotics. Antimicrob. Agents Chemother. 58:6424–6431.

22. Schweizer HP. 2001. Triclosan: a widely used biocide and its link to antibiotics. FEMS Microbiol. Lett. 202:1–7.

23. Chuanchuen R, Beinlich K, Hoang TT, Becher A, Karkhoff-Schweizer RR, Schweizer HP. 2001. Cross-resistance between triclosan and antibiotics in *Pseudomonas aeruginosa* is mediated by multidrug efflux pumps: exposure of a susceptible mutant strain to triclosan selects *nfxB* mutants overexpressing MexCD-OprJ. Antimicrob. Agents Chemother. 45:428–432.

24. Bailey AM, Paulsen IT, Piddock LJ. 2008. RamA confers multidrug resistance in *Salmonella enterica* via increased expression of *acrB*, which is inhibited by chlorpromazine. Antimicrob. Agents Chemother. 52:3604–3611.

25. Yu BJ, Kim JA, Pan JG. 2010. Signature gene expression profile of triclosan-resistant *Escherichia coli.* J. Antimicrob. Chemother. 65:1171–1177.

26. McMurry LM, Oethinger M, Levy SB. 1998a. Triclosan targets lipid synthesis. Nature 394:531–532.

27. Fan F, Yan K, Wallis NG, Reed S, Moore TD, Rittenhouse SF, DeWolf WE, Huang J, McDevitt D, Miller WH, Seefeld MA. 2002. Defining and combating the mechanisms of triclosan resistance in clinical isolates of *Staphylococcus aureus*. Antimicrob. Agents Chemother. 46:3343–3347.

28. Stewart MJ, Parikh S, Xiao G, Tonge PJ, Kisker C. 1999. Structural basis and mechanism of enoyl reductase inhibition by triclosan. J. Mol. Biol. 290:859–865.

29. Campbell JW, Cronan Jr JE. 2001. Bacterial fatty acid biosynthesis: targets for antibacterial drug discovery. Annu. Rev. Microbiol. 55:305–332.

513 30. Khan R, Roy N, Choi K, Lee SW. 2018. Distribution of triclosan-resistant genes in major
514 pathogenic microorganisms revealed by metagenome and genome-wide analysis. PLoS ONE.
515 13:e0192277.

516 31. Sambrook J, Fritsch E, Maniatis T. 1989. Molecular Cloning: a Laboratory Manual, 4th ed,
517 vol 1. Cold Spring Harbor Laboratory Press, New York.

518 32. Sikic K, Carug O. 2010. Protein sequence redundancy reduction: comparison of various
519 method. Bioinformation 5:234–239.

520 33. Tamura K, Stecher G, Peterson D, Filipski A, Kumar S. 2013. MEGA6: molecular
521 evolutionary genetics analysis version 6.0. Mol. Biol. Evol. 30:2725–2729.

522 34. Edgar RC. 2004. MUSCLE: Multiple sequence alignment with high accuracy and high
523 throughput. Nucleic. Acids. Res. 32:1792–1797.

524 35. Yao J, Abdelrahman YM, Robertson RM, Cox JV, Belland RJ, White SW, Rock CO. 2014.
525 Type II fatty acid synthesis is essential for the replication of *Chlamydia trachomatis*. J. Biol.
526 Chem. 289:22365–22376.

527 36. Yoshimoto T, Higashi H, Kanatani A, Lin XS, Nagai H, Oyama H, Kurazono K, Tsuru D.
528 1991. Cloning and sequencing of the 7 alpha-hydroxysteroid dehydrogenase gene from
529 *Escherichia coli* HB101 and characterization of the expressed enzyme. J. Bacteriol.
530 173:2173–2179.

531 37. Egan AF, Russell RR. 1973. Conditional mutations affecting the cell envelope of *Escherichia*
532 *coli* K-12. Genet Res. 21:139–152.

533 38. Chothia C, Lesk AM. 1986. The relation between the divergence of sequence and structure in
534 proteins. EMBO J. 5:823–826.

535 39. Huang J, Rauscher S, Nawrocki G, Ran T, Feig M, de Groot, BL, Grubmuller H, MacKerell
536 AD Jr. 2017. CHARMM36m: an improved force field for folded and intrinsically disordered
537 proteins. Nat. Methods 14:71–73.

538 40. Heath RJ, Rock CO. 1995. Enoyl-acyl carrier protein reductase (*fabI*) plays a determinant
539 role in completing cycles of fatty acid elongation in *Escherichia coli*. J. Biol. Chem.
540 270:26538–26542.

541 41. Heath RJ, Rock CO. 1996. Regulation of fatty acid elongation and initiation by acyl-acyl
542 carrier protein *in Escherichia coli*. J. Biol. Chem. 271:1833–1836.

543 42. Ward WH, Holdgate GA, Rowsell S, McLean EG, Pauptit RA, Clayton E, Nichols WW,
544 Colls JG, Minshull CA, Jude DA, Mistry A. 1999. Kinetic and structural characteristics of
545 the inhibition of enoyl (acyl carrier protein) reductase by triclosan. Biochemistry 38:12514–
546 12525.

547 43. Basso LA, Zheng R, Musser JM, Jacobs WR Jr, Blanchard JS. 1998. Mechanisms of
548 isoniazid resistance in *Mycobacterium tuberculosis*: enzymatic characterization of enoyl
549 reductase mutants identified in isoniazid-resistant clinical isolates. J. Infect. Dis. 178:769–
550 775.

551 44. Xu H, Sullivan TJ, Sekiguchi JI, Kirikae T, Ojima I, Stratton CF, Mao W, Rock FL, Alley
552 MR, Johnson F, Walker SG. 2008. Mechanism and inhibition of saFabI, the enoyl reductase
553 from *Staphylococcus aureus*. Biochemistry 47:4228–42236.

554 45. Ramachandran GN, Ramakrishnan C, Sasisekharan V. 1963. Stereochemistry of polypeptide
555 chain configurations. J. Mol. Biol. 7: 95–99.

46. Wiederstein M, Sippl MJ. 2007. ProSA-web: interactive web service for the recognition of errors in three-dimensional structures of proteins. Nucleic Acids Res. 35:407–410.

47. Kim KH, Ha BH, Kim SJ, Hong SK, Hwang KY, Kim EE. 2011. Crystal structures of enoyl-ACP reductases I (FabI) and III (FabL) from *B. subtilis*. J. Mol. Biol. 406:403–415.

48. Rossmann MG, Moras D, Olsen KW. 1974. Chemical and biological evolution of a nucleotide-binding protein. Nature 250:194–199.

49. Seefeld MA, Miller WH, Newlander KA, Burgess WJ, DeWolf WE, Elkins PA, Head MS, Jakas DR, Janson CA, Keller PM, Manley PJ. 2003. Indole naphthyridinones as inhibitors of bacterial enoyl-ACP reductases FabI and FabK. J. Med. Chem. 46:1627–1635.

50. Kavanagh KL, Jörnvall H, Persson B, Oppermann U. 2008. Medium-and short-chain dehydrogenase/reductase gene and protein families. Cell Mol. Life Sci. 65:3895.

51. Sivaraman S, Sullivan TJ, Johnson F, Novichenok P, Cui G, Simmerling C, Tonge PJ. 2004. Inhibition of the bacterial enoyl reductase FabI by triclosan: a structure− reactivity analysis of FabI inhibition by triclosan analogues. J. Med. Chem. 47:509–518.

52. Qiu X, Abdel-Meguid SS, Janson CA, Court RI, Smyth MG, Payne DJ. 1999. Molecular basis for triclosan activity involves a flipping loop in the active site. Protein Sci. 8:2529–2532.

575 **Figure Legends**

576 **Fig. 1. Bacterial type II fatty acid synthesis (FASII) cycle.** (A) Generalized FASII cycle; Fatty
577 acid biosynthesis is initiated by 3-oxoacyl-acyl carrier protein (ACP) synthase (FabH), which
578 links malonyl-ACP with either acetyl-CoA or 2-methylbutyryl-CoA. The resulting β-ketoacyl-
579 ACP is further reduced by 3-oxoacyl-ACP reductase (FabG), resulting in β-hydroxybutyryl-ACP,
580 which is further dehydrated by 3-hydroxyacyl-ACP dehydratase (FabZ) to produce crotonyl-
581 ACP. The last step in the cycle is the conversion of crotonyl-ACP to acyl-ACP by enoyl-ACP
582 reductase (ENR), which is a target for triclosan activity. (B) ENRs catalyze the reduction
583 reaction.

584

585 **Fig. 2. Phylogenetic analysis of FabL2 ENR and its homologs.** Maximum likelihood analysis
586 was performed with well-characterized 7-AHSDH, FabL, FabV, FabI, and FabK (in bold) and
587 their homologs, with sequence identity >50% using the Uniref50 database. Bootstrap values are
588 shown for each node with >50% support in a bootstrap analysis of 500 replicates. Scale bar
589 represents 0.2 estimated amino acid substitutions per residue.

590

591 **Fig. 3. Biochemical analysis of the metagenomic ENR FabL2.** Initial velocities were
592 determined in triplicates as a function of (A) NADPH concentration and (B) crotonyl-CoA
593 concentration. Data were fitted to the Michaelis–Menten nonlinear regression equation using
594 GraphPad Prism version 7. The fitted line and Km values are shown.

595

596 **Fig. 4. Sequence alignment of FabL2, mutant FabL2 (mFabL2), and template structure.**
597 (A) Sequence alignment of FabL2 and template structure (PDB ID: 3OID), which is the

598 crystallographic structure of *Bacillus subtilis* FabL. The extrapolated mismatched six amino
599 acids comprising the highly flexible loop of FabL2 are shown in red boxes, and the highly
600 conserved catalytic active site residues are shown in magenta boxes. (B) Sequence alignment of
601 mFabL2 and template structure. (C) Complementation analysis of m-FabL2 ENR. Each plate has
602 been divided into three sections: 1, JP111 with pGEM-T Easy only; 2, JP1111 carrying *E. coli*
603 FabI in pGEM-T Easy; 3, JP1111 carrying m-FabL2 in pGEM-T Easy. Plates were incubated at
604 30°C and 42°C for 48 hours.
605
606 **Fig. 5. Homology model and docking of FabL2, mFabL2 and triclosan (TCL).** (A)
607 Molecular dynamic optimized model of FabL2. The α-helices and β-strands are labeled and the
608 extrapolated loop of 7-AHSDH is shown in orange. NDAPH is shown as a stick model. (B)
609 FabL2-TCL complex after docking. TCL is shown as a stick model in magenta; it is bound at the
610 rim region of the tunnel leading to the catalytic site. The size of the tunnel opening is determined
611 by the loop (orange). The putative catalytic site of FabL2 is shown as a sphere (light blue). (C)
612 Two-dimensional (2D) representation of molecular interactions between FabL2 and TCL. Two
613 H-bonds between TCL and the Arg98 residue of FabL2 are shown. (D) Molecular dynamic
614 optimized model of mFabL2. NDAPH is shown as a stick model. (E) mFabL2-TCL complex
615 after docking. TCL is shown as a stick model (magenta), and the putative catalytic site is shown
616 as a sphere (light blue). (F) Two-dimensional (2D) representation of molecular interactions
617 between mFabL2 and TCL after docking. The absence of the extrapolated loop in mFabL2
618 significantly widened the opening of the tunnel leading to the catalytic site of mFabL2. The
619 hydrogen bond is shown as green dashed lines, while the corresponding residue is depicted as
620 green closed circles. (G) 2D representation of mFabL2 and NADPH interactions. All interactions

621 are indicated with dashed lines: H-bonds, black; salt bridge interactions, orange; and other
622 hydrophobic interactions, light magenta. Amino acid residues connected via H-bonds are
623 depicted as green closed circles. All amino acid residues are labeled with their 3-letter code,
624 followed by chain ID in protein structure and their respective amino acid number. (H) Root mean
625 square deviation of Cα-atoms of mFabL2 representing its stability during the simulation. (I)
626 Potential energy of the system, indicating the stability of the mFabL2-TCL complex. (J) Total
627 number of H-bonds between NADPH bound mFabL2 and TCL during the entire simulation
628 period.

[Fig. 1, Raees Khan et al.]

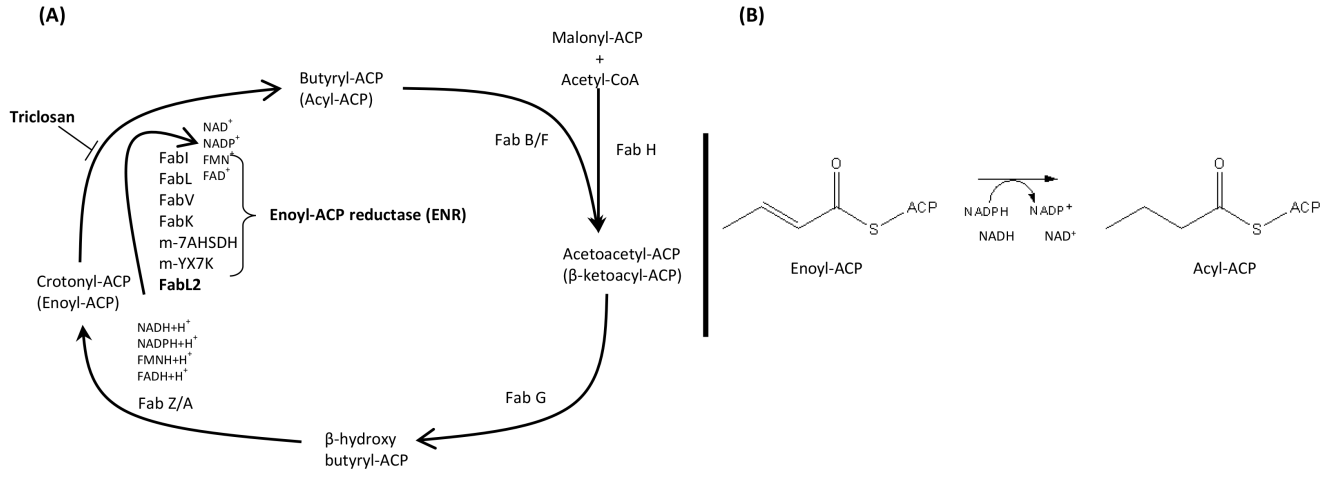

[Fig. 2, Raees Khan et al.]

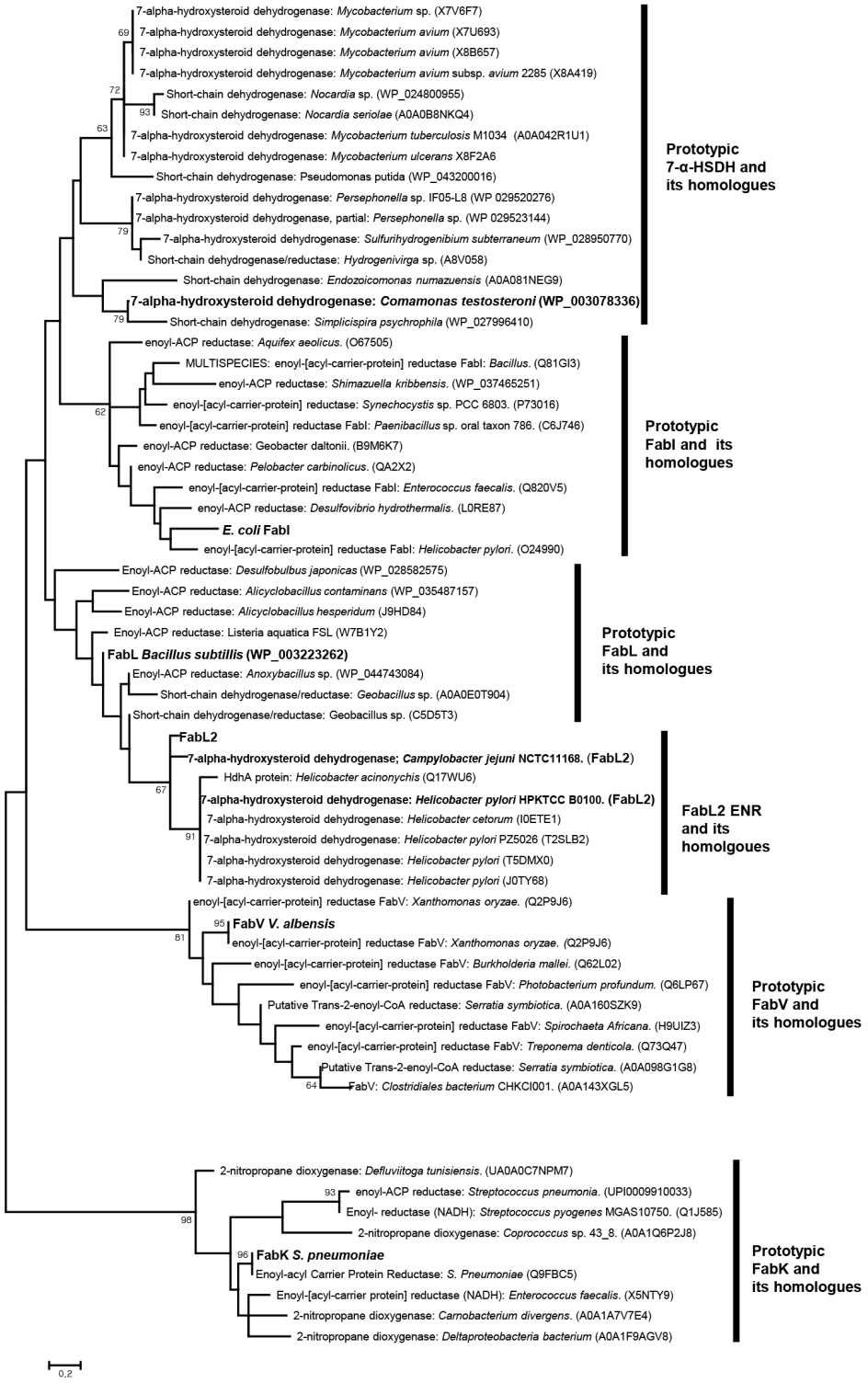

[Fig. 3, Raees Khan et al.]

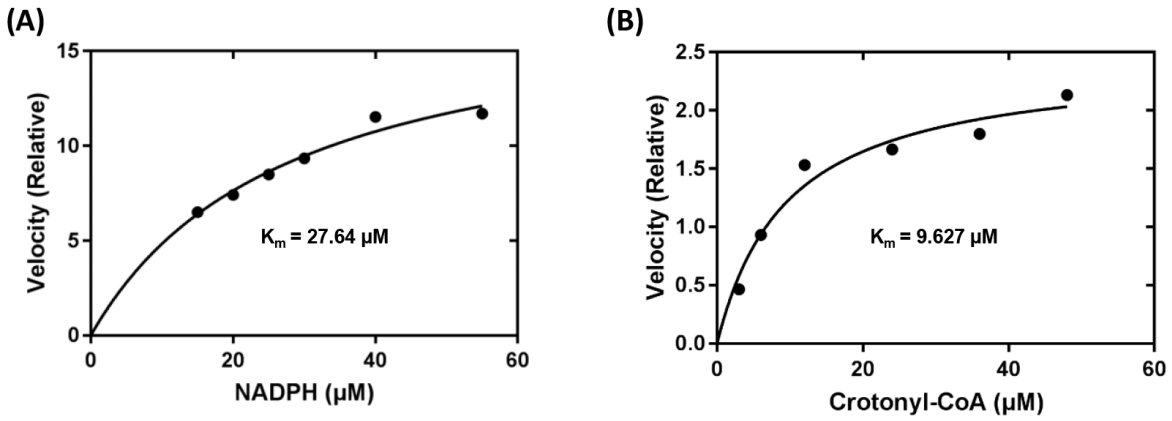

[Fig. 4, Raees Khan et al.]

(A)

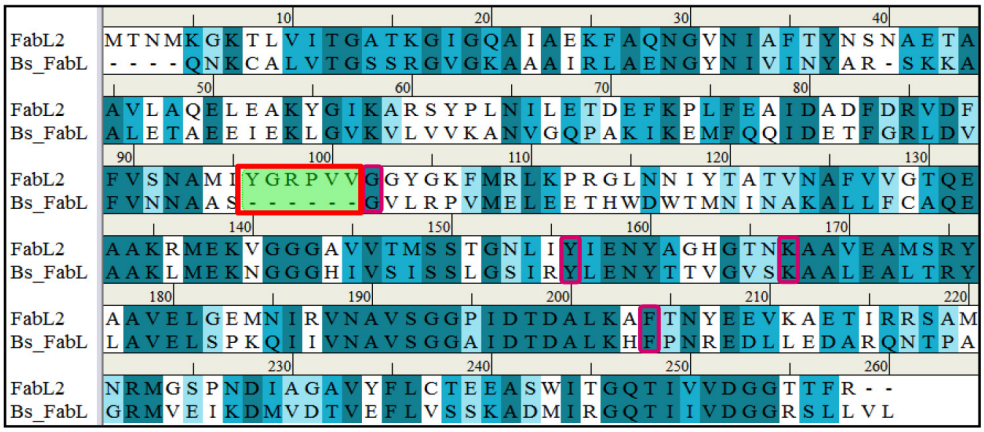

(B)

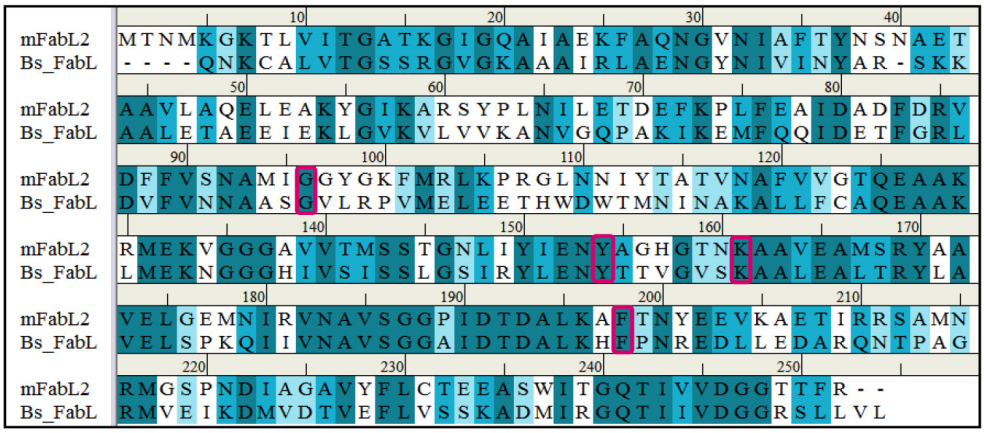

(C)

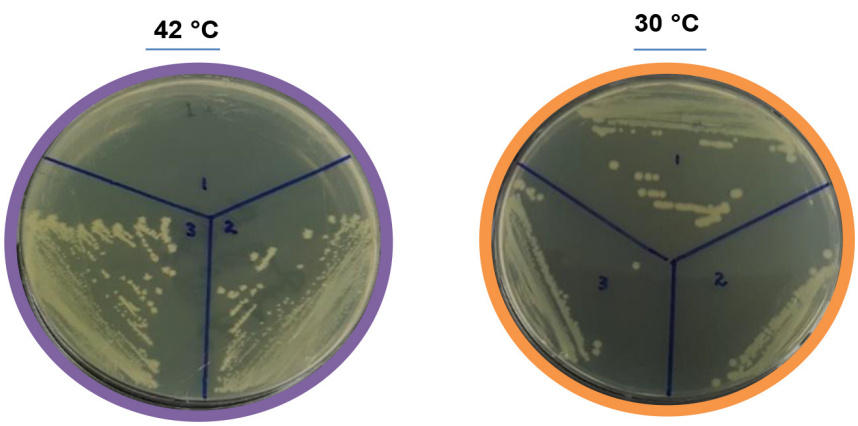

[Fig. 5, Raees Khan et al.]